Science Arts & Métiers (SAM)
is an open access repository that collects the work of Arts et Métiers Institute of Technology researchers and makes it freely available over the web where possible.

This is an author-deposited version published in: https://sam.ensam.eu
Handle ID: .http://hdl.handle.net/10985/18378

To cite this version :

Samira FERNANDES-NASSAR, Nicolas DELPOUVE, Cyrille SOLLOGOUB, Alain GUINAULT, Grégory STOCLET, Sandra DOMENEK, Gilles REGNIER - Impact of Nanoconfinement on Polylactide Crystallization and Gas Barrier Properties - Applied Materials and Interfaces - Vol. 8, n°8, p.9953-9965 - 2020

Any correspondence concerning this service should be sent to the repository Administrator : scienceouverte@ensam.eu

Impact of Nanoconfinement on Polylactide Crystallization and Gas Barrier Properties

Samira Fernandes Nassar, Nicolas Delpouve, Cyrille Sollogoub, Alain Guinault, Gregory Stoclet, Gilles Régnier, and Sandra Domenek*

ABSTRACT: The barrier properties of poly(L-lactide) (PLLA) were investigated in multinanolayer systems, probing the effect of confinement, the compatibility between the confining and the confined polymer, crystal orientation, and amorphous phase properties. The multilayer coextrusion process was used to confine PLLA between two amorphous polymers (polystyrene, PS; and polycarbonate, PC), which have different chemical affinities with PLLA. Confined PLLA layers of approximately 20 nm thickness were obtained. The multinanolayer materials were annealed at different temperatures to obtain PLLA crystallites with distinct polymorphs. PLLA annealed in PC/PLLA films at 120 °C afforded a crystallinity degree up to 65%, and PLLA annealed in PC/PLLA or PS/PLLA films at 85 °C had a crystallinity degree of 45%. WAXS measurements evidenced that the PLLA lamellas between PS layers had a mixed in-plane and on-edge orientation. PLLA lamellas between PC layers were uniquely oriented in-plane. DMA results evidenced a shift of the PC glass transition toward lower temperature, suggesting the possible presence of an interphase. The development of the rigid amorphous fraction (RAF) in the amorphous phase during annealing was impacted by the confiner polymer. The RAF content of semicrystalline PLLA was about 15% in PC/PLLA, whereas it was neglectable in PS/PLLA. The oxygen barrier properties appeared to be governed by RAF content, and no impact of the PLLA polymorph or the crystalline orientation was observed. This study shows that the confinement of PLLA on itself does not impact barrier properties but that the proper choice of the confiner polymer can lead to decrease the phase coupling which creates the RAF. It is the prevention of RAF that decreases permeability.

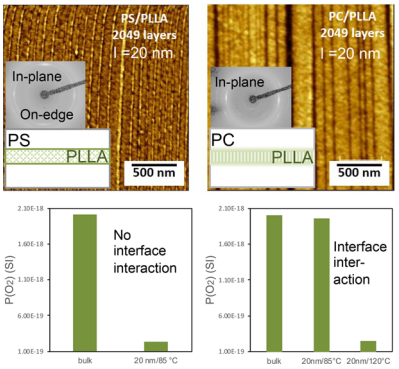

KEYWORDS: *PLLA, confinement, interphase, RAF, permeability*

■ INTRODUCTION

Polylactide (PLA) is today the most produced biodegradable and biobased polymer, mainly used as packaging materials or bioresorbable devices in the biomedical sector.[1] However, compared with other high-performance polymers, its moderate barrier properties hinder larger-scale commercial application. Optimizing PLA barrier properties receives therefore large academic and industrial interest, as attested by the important number of publications summarized in the reviews of Sonchaeng et al.[2] Improvements were often achieved by optimizing crystallization,[3−8] drawing,[9] and compounding or blending with less-permeable polymers or fillers with high aspect ratio.[10,11] However, the decrease in barrier properties is rather limited and generally achieved at the expense of other properties (such as optical clarity, degradability, and mechanical toughness). Alternative strategies must therefore be explored.

Confinement of polymers between hard borders by the multilayer coextrusion process is proposed as a promising technology since the report of a spectacular improvement of oxygen barrier properties of poly(ethylene oxide) (PEO) layers crystallized as single crystals in in-plane orientation between polycaprolactone (PCL) layers.[12] In semicrystalline polymers, crystallization can be profoundly affected by nanoscale confinement:[12] spherulite growth is greatly hampered, and specific lamellar crystal orientations are created. In particular, it was observed that coextruding PEO, PCL or polypropylene (PP) between hard confining layers led to unique single crystalline lamellas oriented parallel to the layers (in-plane).[13−17] Because the impermeable lamellas with large aspect ratios were oriented perpendicularly to the permeant flux, multiple orders of magnitude reduction in gas permeability was achieved compared with the bulk. The orientation of crystals is thus an important parameter, and many reports exist on the subject.[18−23] However, results were often behind expectation.[10,19,22,23] Amorphous-phase dynamics play also a decisive role in the overall barrier properties. In the case of PLA, this was studied in the last years by several

groups[3−5,24] and summarized in the recent review of Sonchaeng et al.[2] However, the impact of confinement of PLA between the hard walls of a second glassy polymer on the barrier properties in such a context has not been studied yet.

Because the control of crystal orientation is crucial for barrier enhancement, a better understanding of the parameters governing the crystalline structuration is needed.[25] The difficulty lies in the fact that it is not a simple task to split the confiner substrate effect from geometrical effects, as well as the effect of crystal growth kinetics from nucleation. The layer multiplying coextrusion appeared as a relevant tool providing insight into the effect of confinement on the crystallization behavior of polymers.[12,16,26] Thermal annealing after extrusion of the confined polymer was used to control the orientation habit. In addition to geometrical confinement (i.e., layer thickness), other parameters were found to impact the lamellar crystal orientation, such as the chemical interaction between confining and confined polymers or the annealing conditions.[12] Besides, with the decrease of the layer thickness, a transition from on-edge lamellas (i.e., lamellas perpendicular to the film layer but polymeric chains parallel to the film layer) to in-plane lamellas (i.e., lamellas parallel to the film layer but polymeric chains perpendicular to the film layer) was observed. A similar transition was found when the (re)crystallization temperature was increased, both on substrate-supported thin films[27,28] and nanolayered films.[21] This transition in orientation was attributed to a transition from heterogeneous nucleation to surface nucleation, being deactivated at high temperatures, suggesting that the lamellar orientation is mainly nucleation controlled.[29]

The substrate effect is still poorly understood. Enhancing polymer−substrate interaction may impose the polymer chains to orient in layer direction, favoring an on-edge lamellar orientation, but some experimental results on substrate-supported thin films contradict this scenario.[27] The substrate effect on the confined crystallization of PCL in coextruded nanolayered films was investigated,[12] and it was shown that increased interaction prevented the formation of in-plane crystalline lamellas. As an attempt to understand the substrate effect, Ma et al.[30−32] performed dynamic Monte Carlo simulations considering two kinds of interactions with the substrate: sticky walls (related to the case of strong adhesion between polymer and wall) and slippery walls (neutral repulsion between polymer and wall). On-edge lamellas were dominant over the whole range of crystallization temperature and film thickness for slippery walls, while for sticky walls in-plane lamellas tended to be dominant.

There are some studies carried out with spin-coated ultrathin PLA films on the influence of annealing temperature on lamellar crystal formation in PLLA. Zhang et al.[33] showed that the confinement of PLLA between polycarbonate (PC) layers decreased the nucleation and crystal growth rates. Wu et al.[34] showed that on-edge lamellar crystals of PLLA thin films are mainly formed by cold crystallization at low temperatures, whereas the in-plane crystals occur when the crystallization temperature approaches 100 °C. However, in another study, Maillard and Prud'homme[35] showed that thin PLLA crystallized at 125 and 160 °C had on-edge lamellas. The conflicting literature results inform that the main factors influencing the orientation of PLA lamella in thin films are still unknown.

In the present work, we investigate the impact of PLLA confinement between slippery or stick walls by polystyrene (PS) or PC on its crystallization behavior, macromolecular mobility, and gas barrier properties. PS and PLLA are immiscible,[36−38] and the different surface tensions[39] of both polymers lead to low compatibility and slippery interfaces. PC and PLA are compatible polymers. Imre et al.[40] showed that up to approximately 5 wt % of PC, the T_g of PLLA increased because of the small admixture. The wall of the confiner polymer PC should as a consequence be stickier for PLLA compared with PS walls. In the aim to discriminate interface and confinement effects, the sample set contained (i) 3-layer PLLA/confiner polymer films as a control, (ii) 513-layer PLLA/confiner polymer films as intermediate condition including a largely multiplied number of interfaces but no confinement, and (iii) 2049-layer PLLA/confiner polymer films with a large number of interfaces and confinement of PLLA. The systematic study of geometrical constraints and compatibility effects will help to deduce engineering rules for increasing the performance of the multilayer materials.

■ MATERIALS AND METHODS

Materials and Processing. Two couples of polymers were used in this study: polylactide (PLLA)/polystyrene (PS) (PS/PLLA) and polylactide (PLLA)/polycarbonate (PC) (PC/PLLA). PLLA pellets were purchased from Corbion Purac (PLA REVODE 190). The content of *L.L*-lactide was higher than 99 mol %. The weight-average molar mass was measured by GPC (Agilent 220 HT) using PS standards. It was equal to M_w = 177 kg mol^{-1} and the dispersity $Đ$, defined as M_w/M_n, was 1.64. The gyration radius of PLLA estimated from the plot of Fang et al.[41] is around 20 nm. Polycarbonate (PC) pellets were obtained from Gazechim (PC121R). Its characteristics were M_n = 19 000 g/mol; M_w = 43 000 g/mol; $Đ$ = 2,4 (done in THF, standards PS). Polystyrene (PS) pellets were purchased from Total Petrochemicals (PS 1340). Its characteristics were M_n = 112 000 g/mol; M_w = 245 000 g/mol; $Đ$ = 2,2 (done in THF, standards PS).

A multilayer coextrusion process was used to elaborate multilayered films composed of 3, 513, and 2049 alternating layers of PLLA and PS or PC. The composition of the multilayer films was 75 wt % confiner polymer and 25 wt % PLLA. In brief, PLLA and PC was dried using a SOMOS dryer (France) with circulation of dry air overnight. The residual humidity of PLLA amounted to 250 to 300 ppm and that of PC was between 150 and 250 ppm. PS was used as received. The experimental setup consisted of two single screw extruders (Rheoscam Scamex, France) of 20 mm with gear pumps, a three-layer feed block (A-B-A), a series of layer-multiplying elements, a flat die, and chill rolls (Scamex, France), as described by our earlier work.[42] The layer-multiplying elements cut the flow in half vertically and subsequently superpose, compress, and stretch it to its original width. A series of n elements leads thus to $2^{n+1}+1$ alternating layers. The extrusion conditions are given in the Supporting Information S.1. In order to ensure the best homogeneity of the layers and to avoid layer breakup, the viscosity ratio should be as close as possible to 1,[43] in the shear rate range of coextrusion process (typically between 1 and 50 s^{-1}). In the case of PC/PLLA, even if the PC grade chosen for this study had a low viscosity, the achieved viscosity ratio in the processing window was around 0.35. In the case of PS/PLLA, a viscosity ratio of 1 was obtained. A graph containing the experimental data is given in the Supporting Information S.2.

In order to obtain films with different nominal individual PLLA layer thickness, the chill roll speed and the number of mixing elements were varied. The target total film thickness to reach a given nominal PLLA layer thickness was calculated taking into account the weight percentage of PLLA and the number of PLLA layers ($l_{PLLA} = 0.25 * l_{film}/_{nPLLA\ layers}$). Using 8 multiplying elements (256 PLLA layers), the total target film thickness is 300 μm and the nominal individual PLLA layer thickness is 300 nm. Using 10 multiplying elements (1024 PLLA layers), the total target film thickness is 80 μm, and the nominal individual PLLA layer thickness 20 nm. Different processing conditions were tested. The following optimized process conditions were employed to reach the target total film thickness

using PS as confiner polymer: 8 multiplying elements and a chill roll of speed 60 cm/min, and 10 multiplying elements and a chill roll speed 200 cm/min. The conditions using PC as confiner polymer were the following: 8 multiplying elements and a chill roll of speed 60 cm/min, and 10 multiplying elements and a chill roll speed of 180 cm/min. The target total film thickness was reached with an experimental variability of approximately 10%. The exact PLLA layer thickness was calculated for each sample taking into account the measured total film thickness. In the aim to simplify the sample nomenclature, we used the nominal layer thickness in the text. To test for variability in oxygen barrier properties caused by changing processing conditions, a broad sample set was used, including the samples produced during process optimization. All corresponding data are shown in Supporting Information S.5.

The crystallization of the PLLA layer was performed subsequently to extrusion, thanks to thermal treatments using a heating press (Darragon, France) to avoid deformation of films due to internal stress release. Rectangular samples of approximately 15 × 20 cm were cut from extruded films, discarding the edges to avoid thickness differences. They were stored in a desiccator over P_2O_5. The samples were then sandwiched between two steel plates lined inside with two Teflon sheets. They were hot-pressed at 85, 100, or 120 °C for 180 min at a pressure of 5×10^6 Pa and cooled under air to room temperature.

Analysis Methods. *Atomic Force Microscopy (AFM).* AFM was used to characterize the layered morphology of the coextruded films. AFM images were obtained in tapping mode using a multimode microscope controlled by a Veeco Nanoscope V controller (France). The tips (silicon, spring constant 40 N/m, oscillation frequency ca. 300 kHz) had a radius of curvature less than 10 nm. Specimens were taken from the center of the extruded films and were cut from the cross section with an ultramicrotome 2088 Ultrotome V (LKB, France) equipped with a diamond knife at a cutting speed of 1 mm·s^{-1}. Fifteen images were recorded at full resolution (4096 × 4096 pixels) with a scan rate of 0.9 Hz throughout the thickness of the film. Following the method developed by Bironeau et al.,[44] the analysis of these 15 images containing each around 20 layers was representative of the whole sample with an variability of 10%.

Wide-Angle X-ray Scattering (WAXS). WAXS data were recorded with the help of a PANanalytical diffractometer (France). The parameters were a beam at 40 kV and 20 mA. The Cu Kα radiation (λ = 1.54 Å) was chosen with a Nickel filter. The WAXS diffractograms were recorded by a CDD camera (Photonic Science, France) in 2-D. WAXS data of crystallization kinetics were recorded with to a Genix microsource (XENOCS, France) equipment operating at 50 kV and 1 mA. The Cu Kα radiation used (l = 1.54 Å) was selected with a curved mirror monochromator. The annealing of the samples was done with a heating plate (Linkam) in situ in the X-ray diffraction machine. Two or three films were stacked in order to increase the WAXS signal and then introduced in a heating stage and heated from the bottom side. Before analysis, standard corrections were applied to the patterns such as dark current subtraction and background correction. The quantification of the crystallinity degree was obtained by subtraction of the signal of the area of the amorphous halo from the total surface area of the diffractogram.

The isothermal crystallization kinetics of PLLA was analyzed with the help of the Avrami equation:

$$\alpha(t) = 1 - \exp(-K \cdot t^n) \tag{1}$$

where $\alpha(t)$ is the relative crystallinity fraction at time t calculated as $\alpha(t)$ = Surface_Peak(t)/Surface_Peak(t_{end}). K is the crystallization rate constant, and n is the Avrami exponent depending on the nucleation and the growth geometry (sphere, disc, etc.).

Modulated Temperature Differential Scanning Calorimetry (MT-DSC). The MT-DSC analyses were performed on a Thermal Analysis Instrument DSC Q100 (TA Instruments, France). Nitrogen was used as the purge gas (50 mL·min^{-1}). Amorphous samples were cut from the extruded films and annealed samples from the hot-pressed films. The sample mass was approximately 5−10 mg. The sample holders were Tzero hermetic aluminum pans. Calibration in temperature and enthalpy was carried out using an Indium standard. Calibration in heat capacity was performed using sapphire as a reference. Heat-only temperature modulation method (oscillation amplitude of 0.32 K, oscillation period of 60 s, and heating rate of 2 K·min^{-1}) was applied to get the content of crystalline and amorphous fractions. The glass transition region of PLLA was specifically investigated using a heat−cool temperature modulation (oscillation amplitude of 3 K, oscillation period of 120 s, and heating rate of 1 K·min^{-1}). Reversing and nonreversing heat flows were obtained from the deconvolution procedure proposed by Reading and coauthors.[45] An example is shown in Supporting Information S.3.

Dynamic Mechanical Thermal Analysis (DMTA). DMTA was carried out on thin film samples (10.25 mm length, 5.00 mm width, and a thickness between 0.08 and 0.12 mm) using a Triton Tritec (France) apparatus operating in dynamic tensile mode. The frequency was set at 1 Hz and the dynamic displacement at 10 μm. The samples were heated from 25 to 200 °C at a heating rate of 2 °C·min^{-1}.

Oxygen Permeability. The oxygen transmission rate was measured with a Systech analyzer 8001 (France) or a Brugger GDP-C (Germany) at 23 °C and 0% RH. Comparative tests on the same samples were done to ensure the equivalence of the results. Oxygen permeability was calculated from the measured oxygen transmission rate (OTR) by multiplying it by the sample thickness (measured with a micrometer on 9 points). For assessing reproducibility, permeability measurements were carried out on at least two different samples obtained by the same protocol. In the Supporting Information S.5, all raw data used for the discussion of the barrier properties are given, including processing conditions, measured total film layer thickness, and calculated nominal PLLA layer thickness.

The permeability of PLLA was calculated using the eq 2 below, derived from the series model for multilayered assemblies. In this equation, 75% by weight of PS or PC and 25% by weight of PLLA are considered:

$$\frac{1}{P_{\text{film}}} = \frac{0.25}{\rho_{\text{PLLA}} \cdot P_{\text{PLLA}}} + \frac{0.75}{\rho_{\text{confiner}} \cdot P_{\text{confiner}}} \tag{2}$$

where PLLA density (ρ_{PLLA}) is 1.25 g/cm^3, PS density (ρ_{PS}) is 1.05 g/cm^3, and PC density (ρ_{PC}) is 1.2 g/cm^3.

RESULTS AND DISCUSSION

Multinanolayer Morphology of PC/PLLA and PS/PLLA Samples. The layer morphology of the sample set, which was achieved by multinanolayer coextrusion process, was verified by means of AFM imaging. Figure 1 shows AFM images for PC/PLLA and PS/PLLA samples using 10 mixing elements (2049 layers). The AFM pictures using 8 mixing elements (513 layers) are shown in the Supporting Information S.4. PC and PS appear bright while PLLA appears dark. The observed PLLA layers of the amorphous samples (Figure 1a,d) were continuous even if some thickness heterogeneities were observed. The PC/PLLA samples (Figure 1d) were more heterogeneous compared with PS/PLLA, probably because of a viscosity ratio of both polymers in the range of 0.3 (Supporting Information S.2). The acquisition of AFM images of PC/PLLA was challenging because of very low contrast and high polarity leading to quick pollution. Few images were obtained, which prevented a complete statistical analysis of the sample. On the basis of a sampling composed of several tens of layers, the measured mean thickness, reported in Table 1, was in a reasonable agreement with the expected nominal thickness. PLLA crystallizes in the α'-form at temperatures lower than 90 °C and in the α-form at temperatures higher than 110 °C. At intermediate temperatures, a mixture of both polymorphs is obtained.[1] To test the effect of the polymorph on the properties of PLLA, low-temperature annealing of PS/PLLA and PC/PLLA at 85 °C was carried out. The high-

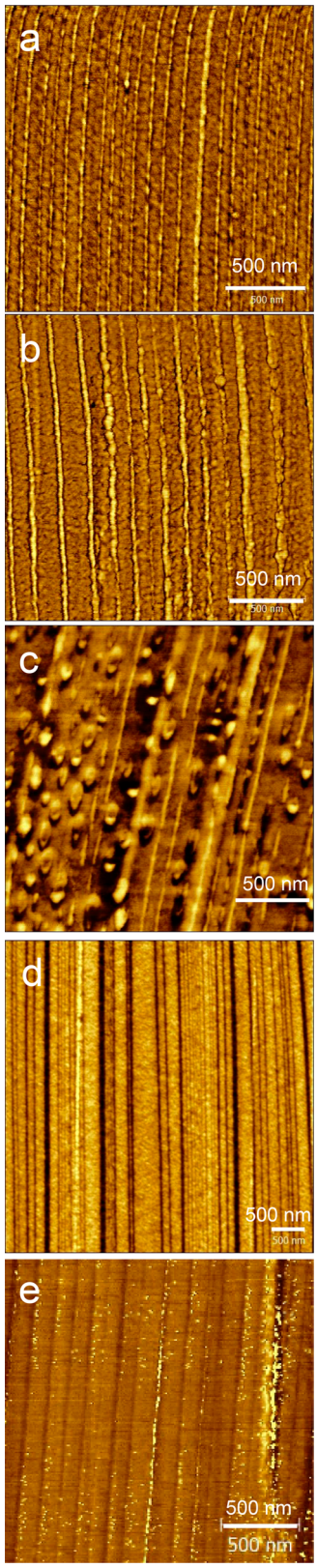

Figure 1. Tapping mode AFM phase image of nanolayered PS/PLLA and PC/PLLA containing 2049 layers. (a) Amorphous PS/PLLA, (b) annealed PS/PLLA 85 °C, (c) annealed PS/PLLA 100 °C, (d) amorphous PC/PLLA, (e) annealed PC/PLLA 120 °C.

temperature annealing of PLLA was limited by the glass transition of PS (T_g = 97 °C). We tested an annealing temperature at 100 °C, in the aim to avoid complete devitrification of the PS layers. Typical AFM pictures of annealed PS/PLLA samples are shown in Figure 1b,c. The crystallization of the PLLA layers at 85 °C (Figure 1b) seemed to induce some supplementary heterogeneities of the layer thickness, but no layer breakup was observed. On the contrary, layer breakup and formation of PLLA droplets were observed after annealing at 100 °C (Figure 1c). We attribute this result to devitrification of PS during the annealing treatment, because the temperature control of the heating press is not very precise and at the beginning of the experiment, heating overshoots can occur which might have increased the effective temperature above T_g of PS. The annealing of PC/PLLA was carried out at temperatures of 85 and 120 °C. The T_g of PC equals to 144 °C; therefore, no layer breakup was suspected. However, because of the better compatibility of PC and PLLA, only very little contrast exists. Therefore, correct AFM pictures of the annealed systems were very difficult to obtain. Only some pictures of annealed PC/PLLA at 120 °C were caught (Figure 1e). We suppose that, in analogy to the PC/PLLA annealed at 120 °C and PS/PLLA annealed at 85 °C, no layer breakup occurred in the PC/PLLA samples during annealing at 85 °C.

Table 1 presents the measured achieved layer thickness of PC/PLLA and PS/PLLA films as a function of extrusion setup.

Table 1. PC/PLLA and PS/PLLA Multilayered Films Used to Study the Effect of PLLA Layer Thickness on the Confinement Effect

multipliers	number of layers	target film thickness (μm)	PLLA nominal thickness (nm)	Measured PLLA thickness in PC (nm)	Measured PLLA thickness in PS (nm)[42]
0	3	120	30000		
8	513	300	300	330 ± 50	220 ± 50
10	2049	80	20	22 ± 5	20 ± 5

Crystallization Kinetics and Crystalline Morphology Confined PLLA Layers. The crystallization kinetics of PLLA under confinement were investigated using in situ WAXS experiments on stacked films. The PS/PLLA system was already presented in our earlier paper.[42] For the sake of comparison, the numerical data are shown together with the analysis of the PC/PLLA system in Table 2. The crystallization kinetics of PLLA between PC layers at 85 and 120 °C are plotted in Figure 2. PLLA crystallization under confinement at 85 °C evolves slower as compared with kinetics of the bulk. This result corresponds to the result obtained under confinement of PLLA in PS.[42] Here, we show that the same behavior is also observed at high crystallization temperature (i.e., 120 °C).

Table 2. Parameters of Isothermal Crystallization with Avrami Model[a]

	$t_{1/2}$ (h)	n	K (h^{-n})
PLLA bulk 85 °C	0.31	3	21.83
PLLA bulk 120 °C	0.1	3	11436
PS/PLLA 20 nm 85 °C[42]	1.84	1.7	0.25
PC/PLLA 20 nm 85 °C	1.54	2	0.28
PC/PLLA 20 nm 120 °C	0.15	2	19.10

[a] $t_{1/2}$: half time; n: Avrami exponent; K: Avrami crystallization rate constant, data of PS/PLLA 20 nm are repeated from our earlier publication, ref 42.

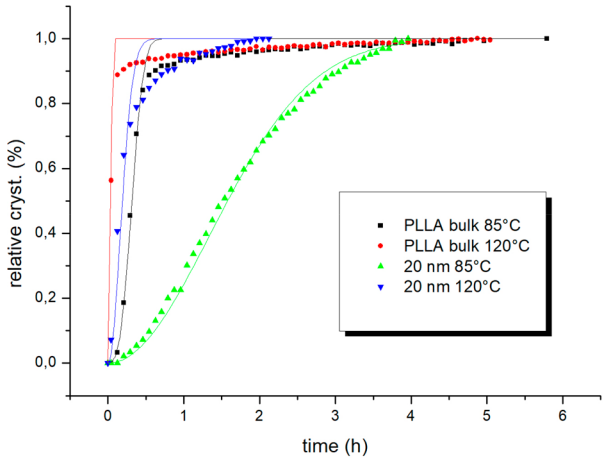

Figure 2. Relative crystallinity and Avrami model (continuous lines) versus crystallization time for isothermal crystallization for bulk PLLA and 20 nm samples at 85 and 120 °C.

The kinetic parameters were modeled with the help of the Avrami theory. The Avrami exponent and the crystallization rate constant were retrieved from the slope and intercept of the linearized crystallization kinetics. While the Avrami exponent of the bulk samples was close to 3, it was somewhat lower than 2 for the confined samples, which approximately corresponds to a two-dimensional crystallization growth with an instantaneous nucleation. The calculated crystallization kinetics (eq 1) are superposed on the experimental data in Figure 2, setting the value of the Avrami constant to 3 for the bulk samples and to 2 for the confined ones. For bulk PLLA and the confined film annealed at 120 °C, nonlinear behavior was observed in the double-logarithmic curve of the Avrami plot ($\ln(-\ln(1-a(t)))$ vs $\ln(t)$, not shown), which suggested the existence of a secondary crystallization.[46] The annealing at 120 °C, that is, close to melting temperature, indeed favored the apparition of the secondary crystallization because macromolecules are more mobile.[46,47] The Avrami model of 20 nm thick PLLA annealed at 85 °C fitted well, and its double-logarithmic curve ($\ln(-\ln(1-a(t)))$ vs $\ln(t)$) was linear. No secondary crystallization was observed. The Avrami parameters of the bulk samples are consistent with literature data.[48]

The half-time of crystallization ($t_{1/2}$) is related to the n and K parameters and was defined as the time at which the extent of relative crystallization reached a value of 50%. Similarly to the results obtained for PLLA confined by PS, half-time crystallization for PLLA confined by PC increased compared with bulk PLLA at 85 °C. K was strongly dependent on the annealing temperature and increased at 120 °C, which was expected from the known behavior of PLLA crystallization in bulk[48] (Table 2).

Figure 3a shows the WAXS intensity profile of the PS/PLLA annealed samples. The extruded samples showed an amorphous halo. The strong reflections of the PLLA crystallites attributed to the (200)/(110) and (203) planes could be observed in samples annealed at 85 °C. Depending on the crystallization temperature, PLLA can crystallize into two distinct polymorphs. Particularly, a low crystallization temperature (i.e., 85 °C) favors the α'-polymorph, while a high temperature (i.e., 120 °C) leads to the α−form.[49−51] These crystalline forms α and α' can be differentiated in the WAXS patterns. A small shift in 2θ values of the two strongest reflections to smaller angles and the appearance of a small reflection at 2θ = 24.8° is characteristic of the α'-form.[52] However, because of the small amount of PLLA in the multilayer samples, the minor reflections characteristics of α'-form at 2θ = 24.8° were not observed. Therefore, the presence of the α' polymorph of PLLA, although likely, cannot be evidenced in PS/PLLA films. Figure 3b shows the WAXS results of PC/PLLA samples. Extruded samples exhibit uniquely an amorphous halo. The annealed films at 85 and 120 °C during 180 min show peaks corresponding to the crystallites of PLLA. The strong reflections of PLLA attributed to the (110)/(200) and (203) planes could be observed in both annealed samples. The strong reflections were shifted to smaller angles in the films annealed at 85 °C, and a very small signal at 2θ = 24.8° was observed. The annealing of the samples PC/PLLA samples at 85 °C yielded thus PLLA crystals in α'-form and the annealing at 120 °C gave rise to the α-polymorph.

The orientation of crystalline lamellas and the crystalline polymorph of extruded and annealed PS/PLLA and PC/PLLA multilayer films were analyzed by WAXS. The WAXS patterns of PS/PLLA films are shown in Figure 4. No arc reflections of crystalline structures were observed in the extruded samples (Figure 4a−c), as they are amorphous. WAXS patterns of 30 μm and 300 nm PS/PLLA films after annealing at 85 °C exhibited isotropic reflection rings from (110)/(200) plane of PLLA (Figure 4d,e). In the case of PS/PLLA 20 nm, crystallization at 85 °C resulted in crystallization forming

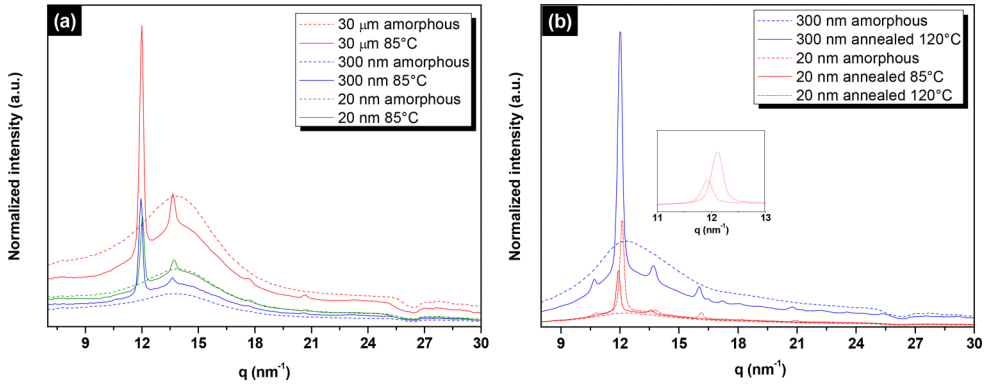

Figure 3. Normalized WAXS intensity profiles of amorphous and annealed PLLA (annealing temperatures 85 and 120 °C, 180 min) as a function of the PLLA layer thickness (30 μm, 300 nm, 20 nm): (a) PS/PLLA system (b) PC/PLLA system. The plot shows an enlarged image of the (110)/(200) plan.

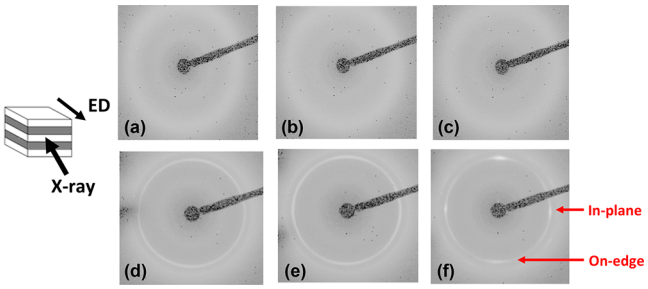

Figure 4. WAXS patterns obtained in extrusion direction (ED) for PS/PLLA (a) 30 μm. (b) 300 nm and (c) 20 nm after extrusion and (d) 30 μm, (e) 300 nm, and (f) 20 nm after annealing at 85 °C during 180 min.

lamellas mainly oriented in both directions, on-edge and in-plane (Figure 4f). The presence of on-edge lamellas was confirmed by meridional reflections for (110)/(200) crystal plane, while in-plane crystals led to the formation of equatorial arcs for the same crystal plane. The formation of mixed lamellas has already been observed on other multilayered films like polypropylene confined by PC[17] or PCL confined by PS/PP.[53]

The WAXS patterns of PC/PLLA films are shown in Figure 5. The extruded films were amorphous. In PC/PLLA films

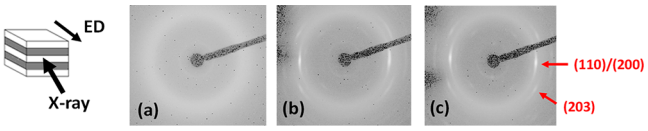

Figure 5. WAXS patterns obtained in extrusion direction (ED) for PC/PLLA samples (a) 20 nm after extrusion, (b) 20 nm after annealing at 85 °C during 180 min, and (c) 20 nm after annealing at 120 °C during 180 min.

with 20 nm PLLA thickness and annealed at 85 and 120 °C, the equatorial reflections for (110)/(200) crystal plane were observed, which indicated the presence of in-plane lamellas. Another evidence for in-plane lamellas in PC/PLLA samples was the reflections at about 30° for the (203) crystal plane. For this crystal plane with in-plane lamellas, and since PLLA has an orthorhombic form[54,55] with parameters a = 1.06 nm, b = 0.610 nm, and c = 2.88 nm,[56] the beam hits lamellas at 60°, reflecting an arc at about 30°.

In conclusion, the confiner polymer influenced apparently the crystalline orientation of PLLA under confinement. Confining PLLA between PS layers induced a mixed orientation of in-plane and on-edge crystals, while PC layers resulted in an in-plane orientation. The same result was obtained notwithstanding the crystallization temperature. The on-edge orientation was observed by different authors as being linked to low crystallization temperatures and homogeneous nucleation,[25,29,34] while in-plane orientation was observed at higher temperatures and in the case of heterogeneous nucleation.[29] At intermediate temperatures, both types of orientation can coexist, which might be the case in the PS/PLLA system. The transition region for the in-plane to on-edge lamellas' orientation was also observed to shift toward lower temperatures for a more interactive system.[12] This may explain why, for similar crystallization temperature (T_c = 85 °C), the more interactive system PC/PLLA leads to only in-plane lamellas, while mixed orientated crystals are present for the noninteracting substrate PS. The higher compatibility of PC with PLLA might facilitate heterogeneous nucleation leading to in-plane crystals.

Microstructure Quantification and Properties of the Amorphous Phases of Confined PLLA. The quantification of crystalline and amorphous fractions in multilayer films from classical DSC needs caution because of the possible superimposition of thermal events in the same temperature domain. This problem can be partly solved by MT-DSC which allows separating two signals, respectively named reversing and nonreversing, the events that only related to the heat capacity change, such as the glass transition, and the kinetic events such as crystallization. Figure 6 shows sample data of the analysis of the films with 20 nm PLLA layer thickness. Figure 6a shows the reversing and nonreversing heat flows of the PS/PLLA film on the example of the amorphous sample with 20 nm layer thickness. The PLLA cold crystallization was partly superposed on the PS glass transition. Likewise, Figure 6b shows that the glass transition of PC is located in the temperature domain where cold crystallization of PLLA ends and melting starts. Therefore, the use of MT-DSC offers a better picture of the glass transition of both confiner and confined polymers.

In the first step, the impact of the both the layer thickness and the PLLA microstructure on the confiner polymer has been assessed. Table 3 contains the quantitative data. Figure 6c shows the zoomed-in graph on the PS glass transition in 20 nm thickness PLLA films. One can observe that the signature of PS glass transition appears noisier when PLLA is amorphous, whereas it is well-defined when PLLA is crystallized at 85 °C, probably because the crystals help to limit the stress relaxation. Independently of PLLA layer thickness and microstructure, no change in the glass transition temperature of PS was observed, evidencing immiscibility between the two polymers (Table 3). According to Table 3, the layer thickness of amorphous PLLA has no obvious influence on the PC glass transition, but Figure 6d shows that the annealing of 20 nm thick PLLA layers induces a broadening of the glass transition. Moreover, when the annealing was performed at 120 °C, T_g of PC slightly decreased. The increase of the layer number caused the increase of the surface area between both polymers, which would enable us to detect the partial miscibility between both polymers. Besides, the annealing at high temperature facilitates the diffusion of one layer into another. The compatibility of PS and PLLA is supposed to be lower than the compatibility between PC and PLLA, which can show partial miscibility.[40] Our hypothesis is that PC interacts strongly enough with PLLA to create an interphase. Another way to evaluate the interpenetration between confiner and confined polymers consists in the determination of the confiner heat capacity step ΔC_p at T_g, then to compare it with the value for a bulk polymer, $\Delta C_{p,bulk}$. Because the composition of the multilayer films is 75 wt % confiner polymer and 25 wt % PLLA, one expects $\Delta C_p/\Delta C_{p,bulk}$ to be close to 75% in the absence of interpenetration, while it would be lower than 75% in the presence of interpenetration. Indeed, the existence of an interphase implies that a part of PC devitrifies between both glass transitions of bulk PC and PLLA. This calculation gives reliable results because both confiners are amorphous. As shown in Table 3, $\Delta C_p/\Delta C_{p,bulk}$ is most often close to, and never below, 75% in PS/PLLA films. The results are more dispersed in the case of PC/PLLA multilayer films. As a consequence, interactions between PC and PLLA are likely,

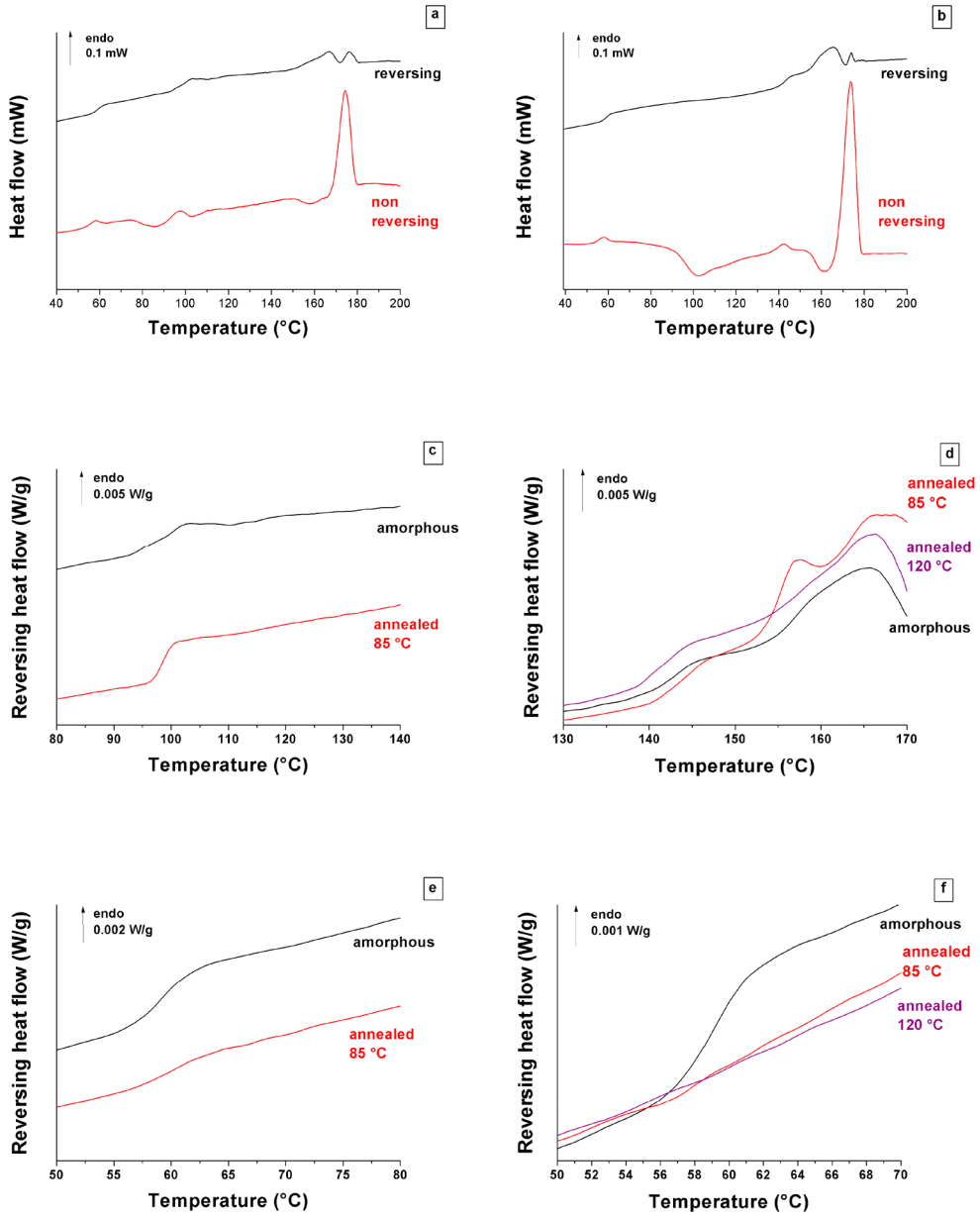

Figure 6. MT-DSC analysis of amorphous and annealed PS/PLLA (left column) and PC/PLLA films with 20 nm thickness (right column). (a) Reversing and nonreversing heat flow of amorphous PS/PLLA (85 °C) recorded with the heat-only protocol; (b) Reversing and nonreversing heat flow of amorphous PC/PLLA (85 °C) recorded with the heat-only protocol; (c) Zoomed-in graph of the glass transition region of PS in amorphous and annealed PS/PLLA films recorded with the heat-only protocol; (d) Zoomed-in graph of the glass transition region of PC in amorphous and annealed PC/PLLA films recorded with the heat-only protocol; (e) Zoomed-in graph of the glass transition region of PLLA in amorphous and annealed PS/PLLA films recorded with the heat−cool protocol; (f) Zoomed-in graph of the glass transition region of PLLA in amorphous and annealed PC/PLLA films recorded with the heat−cool protocol.

but the assumption of an interphase can neither be confirmed nor refuted at this stage.

The impact of confinement on the PLLA microstructure was analyzed with the help of the three-phase model, as previously reported.[4,42] During crystallization, PLLA can develop a rigid amorphous fraction (RAF) in the amorphous phase, which describes coupling between crystalline and amorphous phases by tie chains.[3,4,42,47,57−59] The RAF does not relax at the glass transition of the polymer and is therefore not captured by the height of the heat capacity step at T_g.

The microstructure of the polymer can thus be quantified by

$$X_c + X_{MAF} + X_{RAF} = 1, \text{ with } X_{MAF} = \frac{\Delta C_p}{\Delta C_p^0} \text{ and } X_c = \frac{\Delta H_m - \Delta H_{cc}}{\Delta H_m^0} \quad (3)$$

where X_{MAF} is the content of the mobile (bulk-like) amorphous fraction (MAF) in the amorphous phase, X_c the crystallinity degree, ΔC_p the heat capacity change at glass transition, ΔC_p^0 the heat capacity change at glass transition of the fully amorphous sample, ΔH_m the melting enthalpy, ΔH_{cc} the enthalpy of the cold crystallization, and ΔH_m^0 the melting enthalpy of the perfect crystal at infinite size (93.1 J/g[60]). All

Table 3. Glass Transition Temperature (T_g) of PS and PC in Multinanolayers Films

	T_g (°C)	ΔC_p ($J \cdot g^{-1} \cdot K^{-1}$) of confiner polymer	% of confiner polymer in PLLA/confiner films $\Delta C_p/\Delta C_{p,bulk}$
PS bulk	97 ± 1	0.20 ± 0.01	100
PS/PLLA 300 nm amorphous	97 ± 1	0.16 ± 0.01	78 ± 5
PS/PLLA 300 nm annealed 85°	98 ± 1	0.18 ± 0.02	90 ± 10
PS/PLLA 20 nm amorphous	97 ± 1	0.15 ± 0.01	75 ± 5
PS/PLLA 20 nm annealed 85 °C	98 ± 1	0.15 ± 0.01	75 ± 5
PC bulk	144 ± 1	0.24 ± 0.01	100
PC/PLLA 300 nm amorphous	144 ± 1	0.19 ± 0.03	78 ± 10
PC/PLLA 20 nm amorphous	142 ± 1	0.14 ± 0.02	60 ± 10
PC/PLLA 300 nm annealed 85 °C	144 ± 1	0.13 ± 0.03	52 ± 10
PC/PLLA 300 nm annealed 120 °C	145 ± 1	0.17 ± 0.03	73 ± 10
PC/PLLA 20 nm annealed 85 °C	142 ± 1	0.17 ± 0.02	70 ± 10
PC/PLLA 20 nm annealed 120 °C	140 ± 1	0.17 ± 0.02	72 ± 10

Table 4. Quantification of the Three-Phase Model of PLLA in PS/PLLA and PC/PLLA Multinanolayer Films[a]

	PLLA nominal thickness	T_a (°C)	T_g (°C)	ΔC_p ($J\ g^{1-}K^{-1}$)	X_c (%)	X_{MAF} (%)	X_{RAF} (%)
	PLLA bulk	-	58 ± 1	0.44 ± 0.02	0	100	0
	PLLA bulk	85	67 ± 1	0.19 ± 0.02	51 ± 1	40 ± 2	9 ± 4
	PLLA bulk	120	60 ± 1	0.16 ± 0.02	60 ± 1	36 ± 2	4 ± 4
PS/PLLA[42]	30 000 nm	-	58 ± 1	0.48 ± 0.02	0	100	0
		85	64 ± 1	0.16 ± 0.02	28 ± 2	33 ± 6	39 ± 8
	300 nm	-	58 ± 1	0.44 ± 0.02	0	100	0
		85	66 ± 1	0.20 ± 0.02	36 ± 2	45 ± 6	19 ± 8
	20 nm	-	58 ± 1	0.44 ± 0.02	0	100	0
		85	58 ± 1	0.25 ± 0.02	43 ± 2	57 ± 7	0 ± 9
PC/PLLA	300 nm	-	59 ± 1	0.43 ± 0.10	0	100	0
		85	69 ± 1	0.11 ± 0.10	39 ± 5	25 ± 6	36 ± 8
		120	70 ± 1	0.13 ± 0.10	60 ± 5	30 ± 6	10 ± 8
	20 nm	-	58 ± 1	0.47 ± 0.10	0	100	0
		85	66 ± 3	0.16 ± 0.10	50 ± 5	34 ± 7	16 ± 8
		120	67 ± 3	0.14 ± 0.10	63 ± 5	30 ± 7	7 ± 7

[a] T_a annealing temperature at constant annealing time = 180 min, T_g PLLA glass transition temperature, ΔC_p normalized heat capacity step at T_g to 25% PLLA, X_c crystallinity degree, X_{MAF} quantity of mobile amorphous fraction, X_{RAF} quantity of rigid amorphous fraction. Data of the PS/PLLA systems were published in our earlier work, ref 42.

measured quantities were normalized to the PLLA content of 25 wt %.

The amount of crystallinity of PLLA is given in Table 4. The results of the PS/PLLA system were discussed in our earlier work.[42] We show them here (Figure 6e) for the sake of comparison. The most important conclusion presented in ref 42 says that the confinement of PLLA between noninteracting (slippery) PS walls allowed for crystallizing PLLA with decoupling of amorphous and crystalline phase (0% RAF in the crystallized 20 nm thick films, Table 4). In the confined layers, the RAF did not develop in parallel to the growth of PLLA crystals. This constitutes an important difference to bulk materials, where both phases were shown to develop at the same time.[47]

In the case of sticky walls in the PC/PLLA system, the quantification of the different phases was difficult because of very small signals. It can be observed in Figure 6f, that the glass transition signal of PLLA after annealing almost disappeared. In these conditions, the quantification of MAF and RAF was done using signals obtained from the heat-only protocol (for details, see Supporting Information S.3). However, this calculation cannot consider the possible existence of an interphase between PC and PLLA. The data presented in Table 4 are therefore submitted to high variability. The final crystallinity degree of PLLA crystallized at 120 °C was higher than the one obtained at 85 °C regardless of the layer thickness. This is coherent with established crystallization kinetics of PLLA and with the results obtained by WAXS analysis. Independently of both the layer thickness and the crystallization conditions, the T_g of PLLA clearly shifted to higher temperatures with annealing, showing that the amorphous dynamics are hindered by the adjacent crystalline lamellas. As shown in Table 4, when PLLA crystallizes against PS without forming RAF, no variation of T_g was recorded (see results for 20 nm layer thickness). Therefore, one can expect that the RAF contributes to the mobility restrictions in the amorphous phase of PLLA when crystallized in multilayer films. Here, we cannot clearly evidence an impact of the crystallization temperature on the RAF formation because of the high variability of data. Current literature data including our own work indicate that RAF contents at lower crystallization temperature should be higher, because at low temperature, the hindered mobility of polymer segments affords more coupling points between crystalline and amorphous phase. As a consequence, geometrical limitations increase, which maximizes RAF formation.[4,42,47] Despite the uncertainties, it seems that the RAF development in PC/PLLA is independent from the PLLA layer thickness and that more RAF is created at lower temperature. This is the contrary to the results of the PS/PLLA system reported for the annealed 20

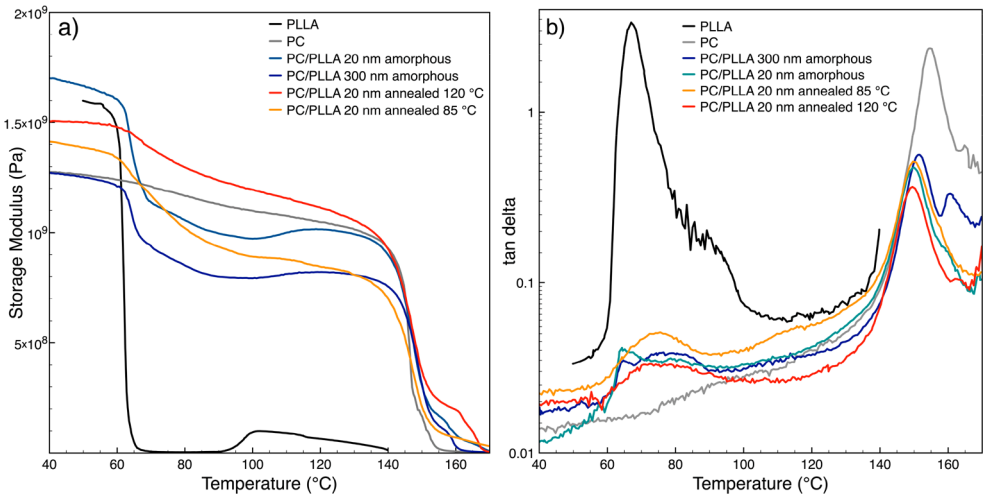

Figure 7. Storage modulus (a) and damping factor (b) of PC and PLLA bulk and amorphous and annealed (85 and 120 °C) PC/PLLA at 300 and 20 nm.

nm thick PLLA layers. We conclude that the interaction of PC walls with PLLA did not allow for the decoupling of the amorphous and crystalline phase when the annealing was carried out at 85 °C.

Dynamic Mechanical Analysis of PC/PLLA. Because of the very small signal of the PLLA glass transition in the PC/PLLA system in MT-DSC leading to high variability, DMA measurements were carried out (Figure 7).

Figure 7a shows the storage modulus E′ of PC/PLLA as a function of temperature. In the aim to magnify differences, a linear scale of E′ is used. PLLA alone shows an important decrease of the elastic modulus upon glass transition and then an increase around 100 °C due to cold crystallization. The multilayer films with PC had higher elastic modulus in the rubbery plateau because PC is in its glassy state. The glass transition of amorphous PLLA in the multilayer films is sudden. It is more gradual but still visible when PLLA was recrystallized. This may correspond to the progressive devitrification of RAF and/or PC/PLLA interphase. Figure 7b shows the tan δ curves of PC/PLLA multinanolayered films. It is possible to observe that the tan δ peak of PC shifted to lower temperatures in the presence of PLLA, which can be attributed to the compatibility between PC and PLLA. In the literature, the appearance of an interphase between PC and PLLA in polymer blends was described and attributed to a transesterification reaction.[61,62] Liu et al.[63] studied the transesterification mechanism between PLA and PC under flow field by adding catalyst to the PLA/PC blend. They found that the transesterification reaction between PLA and PC could occur even without catalyst.

Impact of PLLA Confinement on Oxygen Barrier Properties. Table 5 reports the oxygen permeability of PS/PLLA and PC/PLLA films. The multilayer films containing PLLA had better barrier properties than the PS or PC films, behavior which was expected because PLLA has lower permeability to O_2 than PS and PC. The gain in overall barrier properties of the different systems compared with the properties of the confiner polymer is reported in Table 5. The fully amorphous systems showed an increase in O_2 barrier properties by a factor 2, when PLLA was combined with PS or PC. The crystallization of the PLLA layers permitted gains up to a factor 12 for PS and to a factor 8 for PC.

Table 5. Oxygen Permeability of PS/PLLA and PC/PLLA Films and the Gain of Barrier Properties with Respect to the Confiner Polymer

	PLLA nominal thickness	T_a (°C)	t_a (min)	$P(O_2) \times 10^{-18}$ ($m^3 \cdot m \cdot m^{-2} \cdot s^{-1} \cdot Pa^{-1}$)	gain[a]
	PS bulk			15.3 ± 0.2	
	PC bulk			10.1 ± 0.1	
	PLLA bulk	-	-	2.4 ± 0.5	
	PLLA bulk	85	180	2.2 ± 0.3	
	PLLA bulk	120	180	0.43 ± 0.01	
PS/PLLA	300 nm	-	-	7.8 ± 0.8	2
	300 nm	85	180	4.2 ± 0.5	3
	20 nm	-	-	6.6 ± 0.3	2
	20 nm	85	180	1.3 ± 0.2	12
	20 nm	100	180	12.6 ± 0.8	1.2
PC/PLLA	300 nm	-	-	5.6 ± 0.7	2
	300 nm	85	180	11	none
	300 nm	120	180	1.3 ± 0.1	8
	20 nm	-	-	4.6 ± 0.3	2
	20 nm	85	180	6.5 ± 0.5	1.5
	20 nm	120	180	1.3 ± 0.1	8

[a]gain = ($P_{confiner}/P_{multilayer}$)

To investigate the property change of the confined PLLA layers, we used the law of serial resistances (eq 2) for the calculation of the permeability of PLLA. The implicit hypothesis is that the barrier properties of the confiner polymers PS and PC are constant. This hypothesis is commonly used in the study of multilayer films.[19,22]

Figure 8 shows the whole permeability data set in the aim to picture the evolution of the barrier properties with changing PLLA microstructure (both crystalline and amorphous phases). The exact conditions and numerical data of each point are shown in the Supporting Information S.5.

Amorphous Samples. The inspection of PS/PLLA data shows that the PLLA barrier properties of the amorphous samples were equal to the bulk data, regardless of the PLLA layer thickness and processing conditions. The obtained values correspond to usually reported data.[2] The barrier properties of PLLA layers of 300 nm thickness between PC layers were equal to the bulk value. Interestingly, a small decrease in $P(O_2)$

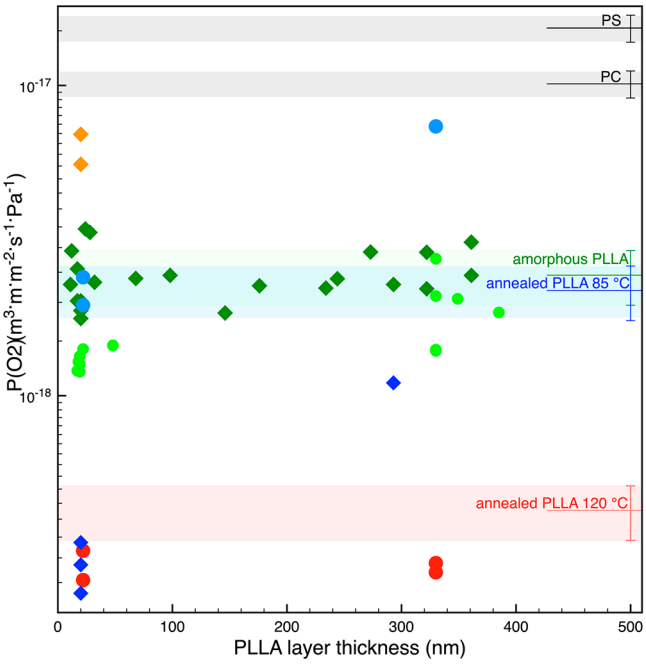

Figure 8. Oxygen permeability of PLLA in PS/PLLA (♦) and PC/PLLA (●) films in comparison to the permeability data of the bulk materials (annealing time 180 min). The annealing conditions are distinguished by the color of the symbols: amorphous PLLA green ◆, light-green ●; annealed PLLA at 85 °C for 180 min between PS layers (blue ◆), between PC layers (light-blue ●); annealed PLLA at 100 °C for 180 min between PS layers (orange ◆), annealed at 120 °C for 180 min between PC layers (red ●). The value of the bulk materials is indicated as a colored range corresponding to the variability interval. It used the properties measured in the actual study and the ones measured in our earlier study (ref 4).

was observed at 20 nm layer thickness. This might be an effect of the interface compatibility.

Annealed PS/PLLA Films. The more interesting results are obtained after the annealing of the PLLA layers. The $P(O_2)$ of the annealed 300 nm layers was lower than the one of the annealed bulk sample. Surprisingly, the $P(O_2)$ of PLLA in 20 nm thick layers was lowered by 1 order of magnitude compared with the bulk and even better than the results obtained with high-temperature annealing, although the crystallinity degree was lower (43 vs 60%, Table 4), and no homogeneous orientation of crystalline lamellas perpendicular to the gas permeation direction was obtained (Figure 4). The PS/PLLA-20 nm sample showed crystallization kinetics without secondary crystallization, changed Avrami exponents, and most importantly, no occurrence of RAF within the experimental uncertainty (Table 2 and 4, ref 42). We conclude therefore that the change in crystalline organization leading to a negligible amount of RAF caused the important improvement of PLLA barrier properties. An interesting result for choosing annealing process parameters of confined PLLA was obtained using a treatment at 100 °C. This temperature was chosen in the aim to obtain a different PLLA polymorph, but it fell in the glass transition region of the confiner polymer. In that case, the barrier properties decreased, most probably due to layer breakup (see Figure 1 and Supporting Information S.5, Table S.4). A conclusion is that the confiner polymer needs to be glassy during the annealing treatment to be able to stabilize the structure.

Annealed PC/PLLA Films. PC/PLLA had a different behavior than PS/PLLA. The PLLA layers annealed at 85 °C did not show any increase of barrier properties compared to the bulk, although the crystalline orientation in the 20 nm thick films was in-plane. Table 4 shows that there the quantity of RAF in PC/PLLA annealed at 85 °C was superior to the bulk sample. In particular, it was very high in the PC/PLLA-300 nm films which had also high permeability (Figure 8). Moreover, the RAF quantity in the PC/PLLA-20 nm was apparently higher than in PS/PLLA. This can be observed looking at the very broad glass transition (Figure 6), although the quantitative determination was subject to uncertainty (Table 4). This is a clear impact of the properties of the confiner polymer and a possible interphase. This result shows again that the crystalline in-plane orientation alone was not enough to increase the barrier properties, but that the RAF is detrimental to the barrier properties of the PC/PLLA crystallized at 85 °C. It could be opposed to this reasoning that the annealing treatment at 120 °C yielded a substantial gain in barrier properties (Figure 8), although RAF formed in PC/PLLA when crystallizing at 120 °C. It is worth mentioning that the percentage of RAF was lower compared with the treatment at 85 °C, even if variability was high. Moreover, the observed permeability values were hardly lower than what can be obtained by cold crystallization of the bulk at high temperature without RAF. Our hypothesis to explain this result is that the crystallites, despite the high crystallinity degree and in-plane orientation (Figure 5), might not overlap enough or be large enough to induce an important tortuosity on the diffusive pathway. It is also interesting to question whether the RAF could differently impact the barrier properties depending on its temperature of formation. The temperature of RAF devitrification, which ranges between the glass transition and the melting temperature, indicates its level of ordering.[47] In bulk conditions, the stack model can be used to describe the organization of crystalline lamellas and the location of RAF. Righetti et al.[64] proposed that the PLA crystallites can be described with the heterogeneous stack model as its glass transition increases with decreasing the crystallization temperature. This implies that the RAF is selectively positioned between lamellas and MAF between the stacks. As previously mentioned, the change in the Avrami parameters when confining PLLA in the multilayer structure suggests a different crystalline organization. A hypothesis would be that in the case of nonoverlapping lamellas, RAF adjacent to the crystalline phase does impact notably on the diffusive pathway. In the PC/PLLA multilayer films crystallized at 85 and 120 °C, the uncertainties around the glass transition are too high to discuss its evolution with the crystallization temperature. To summarize, the negative impact of the RAF on barrier properties is clearly assessed, but a quantitative relationship cannot be given today.

■ CONCLUSIONS

The innovative layer multiplying coextrusion process allowed the fabrication of multilayered films composed of alternating layers of PLLA and an amorphous polymer (PS or PC). Continuous layers with individual thicknesses of PLLA down to 20 nm were obtained. The study of those films extended our insights into PLLA crystallization under confinement. In particular, by choosing two amorphous polymers (PS and PC) having different chemical affinities with PLLA, the role of the confining polymer was investigated.

While the as-extruded films contained amorphous PLLA layers, high degrees of crystallinity were achieved by thermal annealing at temperatures below the glass transition of the confining polymer. Highly orientated lamellas were obtained having in-plane orientation in the PC/PLLA samples and mixed in-plane and on-edge orientation in the PS/PLLA samples. This suggests that a higher interaction between the two polymers can favor the formation of in-plane lamellas. The quantitative study of the amorphous and crystalline phases in PS/PLLA and PC/PLLA films showed that decoupling of amorphous and crystalline phases characterized by low RAF during annealing at low temperature was only possible when the confiner polymer had low interaction with the PLLA layers. The occurrence of RAF in PC/PLLA samples had a negative impact on the barrier properties of the films, which could not be attenuated by the presence of in-plane crystals. More interestingly, annealing PS/PLLA films to obtain a high crystallinity degree without RAF allowed for a barrier improvement of the PLLA layers by a factor of 10 compared with amorphous PLLA. This was 2 times better than semicrystalline bulk PLLA. This unique result informs on the impact of the phase coupling on the PLLA barrier properties and on what properties can be probably achieved by nonoriented crystallization of PLA.

The exact processing parameters to obtain the mulit-nanolayer films (S.1), the analysis of the viscosity ratio of PC and PLLA (S.2), MT-DSC protocols with an example of data treatment (S.3), supplementary AFM pictures (S.4), numerical data of the oxygen permeability of each sample used in Figure 8 (S.5) (PDF)

AUTHOR INFORMATION

Corresponding Author

Sandra Domenek − *Université Paris-Saclay, AgroParisTech, INRAE, UMR 0782 SayFood, 91300 Massy, France;* orcid.org/0000-0003-3012-041X; Email: sandra.domenek@agroparistech.fr

Authors

Samira Fernandes Nassar − *Université Paris-Saclay, AgroParisTech, INRAE, UMR 0782 SayFood, 91300 Massy, France*

Nicolas Delpouve − *Normandie Univ, UNIROUEN Normandie, INSA Rouen, CNRS, Groupe de Physique des Matériaux, 76000 Rouen, France;* orcid.org/0000-0002-6064-7151

Cyrille Sollogoub − *Laboratoire PIMM, Arts et Métiers, CNRS, CNAM, Hesam Université, F-75013 Paris Cedex, France;* orcid.org/0000-0003-2204-3696

Alain Guinault − *Laboratoire PIMM, Arts et Métiers, CNRS, CNAM, Hesam Université, F-75013 Paris Cedex, France*

Gregory Stoclet − *Univ Lille, CNRS, INRA, ENSCL, UMR 8207 - UMET - Unité Matériaux et Transformations, F-59000 Lille, France;* orcid.org/0000-0003-1510-0234

Gilles Régnier − *Laboratoire PIMM, Arts et Métiers, CNRS, CNAM, Hesam Université, F-75013 Paris Cedex, France*

Notes

The authors declare no competing financial interest.

ACKNOWLEDGMENTS

The authors acknowledge the Ph.D. grant CAPES n°9712-13-5 for Samira Fernandes Nassar. Furthermore, they acknowledge the technical help of Flavien Lecourtier (INRAE) for the measurement of the oxygen permeability.

REFERENCES

(1) Ducruet, V.; Domenek, S. Characteristics and Applications of Poly(lactic acid). In *Biodegradable and Bio-Based Polymers: Environmental and Biomedical Applications*, Kalia, S.; Averous, L., Eds.; Scrivener Publishing LLC: Beverly, MA, 2015; Chapter 6, pp 171−224.

(2) Sonchaeng, U.; Iniguez-Franco, F.; Auras, R.; Selke, S.; Rubino, M.; Lim, L. T. Poly(lactic Acid) Mass Transfer Properties. *Prog. Polym. Sci.* **2018**, *86*, 85−121.

(3) Guinault, A.; Sollogoub, C.; Ducruet, V.; Domenek, S. Impact of Crystallinity of Poly(lactide) on Helium and Oxygen Barrier Properties. *Eur. Polym. J.* **2012**, *48* (4), 779−788.

(4) Nassar, S. F.; Guinault, A.; Delpouve, N.; Divry, V.; Ducruet, V.; Sollogoub, C.; Domenek, S. Multi-Scale Analysis of the Impact of Polylactide Morphology on Gas Barrier Properties. *Polymer* **2017**, *108*, 163−172.

(5) Cocca, M.; Di Lorenzo, M. L.; Malinconico, M.; Frezza, V. Influence of Crystal Polymorphism on Mechanical and Barrier Properties of Poly(L-lactic Acid). *Eur. Polym. J.* **2011**, *47*, 1073−1080.

(6) Drieskens, M.; Peeters, R.; Mullens, J.; Franco, D.; Lemstra, P. J.; Hristova-Bogaerds, D. G. Structure Versus Properties Relationship of Poly(lactic Acid). I. Effect of Crystallinity on Barrier Properties. *J. Polym. Sci., Part B: Polym. Phys.* **2009**, *47* (22), 2247−2258.

(7) Courgneau, C.; Domenek, S.; Lebosse, R.; Guinault, A.; Averous, L.; Ducruet, V. Effect of Crystallization on Barrier Properties of Formulated Polylactide. *Polym. Int.* **2012**, *61* (2), 180−189.

(8) Colomines, G.; Ducruet, V.; Courgneau, C.; Guinault, A.; Domenek, S. Barrier Properties of Poly(lactic Acid) and its Morphological Changes Induced by Aroma Compound Sorption. *Polym. Int.* **2010**, *59* (6), 818−826.

(9) Delpouve, N.; Stoclet, G.; Saiter, A.; Dargent, E.; Marais, S. Water Barrier Properties in Biaxially Drawn Poly(lactic Acid) Films. *J. Phys. Chem. B* **2012**, *116* (15), 4615−4625.

(10) Boufarguine, M.; Guinault, A.; Miquelard-Garnier, G.; Sollogoub, C. PLA/PHBV Films with Improved Mechanical and Gas Barrier Properties. *Macromol. Mater. Eng.* **2012**, *298* (10), 1065−1073.

(11) Picard, E.; Espuche, E.; Fulchiron, R. Effect of an Organo-Modified Montmorillonite on PLA Crystallization and Gas Barrier Properties. *Appl. Clay Sci.* **2011**, *53* (1), 58−65.

(12) Carr, J. M.; Langhe, D. S.; Ponting, M. T.; Hiltner, A.; Baer, E. Confined Crystallization in Polymer Nanolayered Films: A Review. *J. Mater. Res.* **2012**, *27* (10), 1326−1350.

(13) Wang, H.; Keum, J. K.; Hiltner, A.; Baer, E. Confined Crystallization of PEO in Nanolayered Films Impacting Structure and Oxygen Permeability. *Macromolecules* **2009**, *42* (18), 7055−7066.

(14) Wang, H.; Keum, J. K.; Hiltner, A.; Baer, E.; Freeman, B.; Rozanski, A.; Galeski, A. Confined Crystallization of Polyethylene Oxide in Nanolayer Assemblies. *Science* **2009**, *323* (5915), 757−760.

(15) Zhang, G. J.; Baer, E.; Hiltner, A. Gas Permeability of Poly(4-Methylpentene-1) in a Confined Nanolayered Film System. *Polymer* **2013**, *54* (16), 4298−4308.

(16) Ponting, M.; Lin, Y. J.; Keum, J. K.; Hiltner, A.; Baer, E. Effect of Substrate on the Isothermal Crystallization Kinetics of Confined Poly(Epsilon-Caprolactone) Nano Layers. *Macromolecules* **2010**, *43* (20), 8619−8627.

(17) Langhe, D. S.; Hiltner, A.; Baer, E. Melt Crystallization of Syndiotactic Polypropylene in Nanolayer Confinement Impacting Structure. *Polymer* **2011**, *52* (25), 5879−5889.
(18) Yu, F. L.; Deng, H.; Bai, H. W.; Zhang, Q.; Wang, K.; Chen, F.; Fu, Q. Confine Clay in an Alternating Multi Layered Structure through Injection Molding: A Simple and Efficient Route to Improve Barrier Performance of Polymeric Materials. *ACS Appl. Mater. Interfaces* **2015**, *7* (19), 10178−10189.
(19) Carr, J. M.; Mackey, M.; Flandin, L.; Hiltner, A.; Baer, E. Structure and Transport Properties of Polyethylene Terephthalate and Poly(Vinylidene Fluoride-Co-Tetrafluoroethylene) Multilayer Films. *Polymer* **2013**, *54* (6), 1679−1690.
(20) Zhang, G. J.; Xu, H.; Macinnis, K.; Baer, E. Crystallization of Linear Low Density Polyethylene under Two-Dimensional Confinement in High Barrier Blend Systems. *Polymer* **2014**, *55* (26), 6853−6860.
(21) Zhang, G. J.; Lee, P. C.; Jenkins, S.; Dooley, J.; Baer, E. The Effect of Confined Spherulite Morphology of High-Density Polyethylene and Polypropylene on Their Gas Barrier Properties in Multilayered Film Systems. *Polymer* **2014**, *55* (17), 4521−4530.
(22) Messin, T.; Marais, S.; Follain, N.; Chappey, C.; Guinault, A.; Miquelard-Garnier, G.; Delpouve, N.; Gaucher, V.; Sollogoub, C. Impact of of Water and Thermal Induced Crystallizations in A PC/MXD6Multilayer Film on Barrier Properties. *Eur. Polym. J.* **2019**, *111*, 152−160.
(23) Su, H. J.; Xue, J.; Cai, P. L.; Li, J.; Guo, S. Y. Structure and Oxygen-Barrier Properties of (Linear Low-Density Polyethylene/Ethylene-Vinyl Alcohol Copolymer)/Linear Low-Density Polyethylene Composite Films Prepared by Microlayer Coextrusion. *J. Appl. Polym. Sci.* **2015**, *132* (27), 42211.
(24) Delpouve, N.; Delbreilh, L.; Stoclet, G.; Saiter, A.; Dargent, E. Structural Dependence of The Molecular Mobility in The Amorphous Fractions of Polylactide. *Macromolecules* **2014**, *47* (15), 5186−5197.
(25) Wang, Y.; Chan, C. M.; Ng, K. M.; Li, L. What Controls The Lamellar Orientation At The Surface of Polymer Films During Crystallization? *Macromolecules* **2008**, *41* (7), 2548−2553.
(26) Michell, R. M.; Muller, A. J. Confined Crystallization of Polymeric Materials. *Prog. Polym. Sci.* **2016**, *54*−*55*, 183−213.
(27) Liu, Y. X.; Chen, E. Q. Polymer Crystallization of Ultrathin Films on Solid Substrates. *Coord. Chem. Rev.* **2010**, *254* (9−10), 1011−1037.
(28) Prud'homme, R. E. Crystallization and Morphology of Ultrathin Films of Homopolymers and Polymer Blends. *Prog. Polym. Sci.* **2016**, *54*−*55*, 214−231.
(29) Wang, H. P.; Keum, J. K.; Hiltner, A.; Baer, E. Impact of Nanoscale Confinement on Crystal Orientation of Poly(Ethylene Oxide). *Macromol. Rapid Commun.* **2010**, *31* (4), 356−361.
(30) Ma, Y.; Hu, W. B.; Hobbs, J.; Reiter, G. Understanding Crystal Orientation in Quasi-One-Dimensional Polymer Systems. *Soft Matter* **2008**, *4* (3), 540−543.
(31) Hu, W. B.; Cai, T.; Ma, Y.; Hobbs, J. K.; Farrance, O.; Reiter, G. Polymer Crystallization Under Nano-Confinement of Droplets Studied by Molecular Simulations. *Faraday Discuss.* **2009**, *143*, 129−141.
(32) Ma, Y.; Hu, W. B.; Reiter, G. Lamellar Crystal Orientations Biased by Crystallization Kinetics in Polymer Thin Films. *Macromolecules* **2006**, *39* (15), 5159−5164.
(33) Zhang, R. C.; Huang, Z. H.; Sun, D.; Lu, A.; Zhong, M. L.; Fang, Z. X.; Ji, D. H.; Xiong, G. Y.; Wan, Y. Z. Crystallization of Poly(L-Lactide) in A Confined Space Between Polycarbonate Layers. *J. Polym. Mater.* **2018**, *35* (2), 171−179.
(34) Wu, N. J.; Ding, M. C.; Li, C. W.; Yuan, Y.; Zhang, J. M. Lamellar Orientation and Crystallization Dynamics of Poly (L-lactic Acid) Thin Films Investigated by In-Situ Reflection Absorption Infrared Spectroscopy. *J. Phys. Chem. B* **2011**, *115* (40), 11548−11553.
(35) Maillard, D.; Prud'Homme, R. E. Crystallization of Ultrathin Films of Polylactides: From Chain Chirality to Lamellar Curvature and Twisting. *Macromolecules* **2008**, *41*, 1705−1712.
(36) Mohamed, A.; Gordon, S. H.; Biresaw, G. Poly(lactic Acid)/Polystyrene Bioblends Characterized by Thermogravimetric Analysis, Differential Scanning Calorimetry, and Photoacoustic Infrared Spectroscopy. *J. Appl. Polym. Sci.* **2007**, *106* (3), 1689−1696.
(37) Leung, B. O.; Hitchcock, A. P.; Brash, J. L.; Scholl, A.; Doran, A. Phase Segregation in Polystyrene-Polylactide Blends. *Macromolecules* **2009**, *42* (5), 1679−1684.
(38) Sarazin, P.; Favis, B. D. Morphology Control in Co-Continuous Poly(L-Lactide)/Polystyrene Blends: A Route towards Highly Structured and Interconnected Porosity in Poly(L-Lactide) Materials. *Biomacromolecules* **2003**, *4* (6), 1669−1679.
(39) Biresaw, G.; Carriere, C. J. Interfacial Tension of Poly(lactic Acid)/Polystyrene Blends. *J. Polym. Sci., Part B: Polym. Phys.* **2002**, *40* (19), 2248−2258.
(40) Imre, B.; Renner, K.; Pukanszky, B. Interactions, Structure and Properties in Poly(lactic acid)/Thermoplastic Polymer Blends. *eXPRESS Polym. Lett.* **2014**, *8* (1), 2−14.
(41) Fang, H.; Zhang, Y.; Bai, J.; Wang, Z.; Wang, Z. Bimodal Architecture and Rheological and Foaming Properties for Gamma-Irradiated Long-Chain Branched Polylactides. *RSC Adv.* **2013**, *3* (23), 8783−8795.
(42) Nassar, S. F.; Domenek, S.; Guinault, A.; Stoclet, G.; Delpouve, N.; Sollogoub, C. Structural and Dynamic Heterogeneity in the Amorphous Phase of Poly(L,L-Lactide) Confined at the Nanoscale by the Coextrusion Process. *Macromolecules* **2018**, *51* (1), 128−136.
(43) Bironeau, A.; Salez, T.; Miquelard-Garnier, G.; Sollogoub, C. Existence of a Critical Layer Thickness in PS/PMMA Nanolayered Films. *Macromolecules* **2017**, *50* (10), 4064−4073.
(44) Bironeau, A.; Dirrenberger, J.; Sollogoub, C.; Miquelard-Garnier, G.; Roland, S. Evaluation of Morphological Representative Sample Sizes for Nanolayered Polymer Blends. *J. Microsc.* **2016**, *264* (1), 48−58.
(45) Reading, M.; Hourston, D. *Theory and Practice of Modulated Temperature Differential Scanning Calorimetry*; Springer: Berlin, 2006.
(46) Park, S. H.; Lee, S. G.; Kim, S. H. Isothermal Crystallization Behavior and Mechanical Properties of Polylactide/Carbon Nanotube Nanocomposites. Compos. *Composites, Part A* **2013**, *46*, 11−18.
(47) Righetti, M. C.; Tombari, E. Crystalline, Mobile Amorphous and Rigid Amorphous Fractions in Poly(L-lactic acid) by TMDSC. *Thermochim. Acta* **2011**, *522* (1−2), 118−127.
(48) Saeidlou, S.; Huneault, M. A.; Li, H.; Park, C. B. Poly(lactic acid) Crystallization. *Prog. Polym. Sci.* **2012**, *37*, 1657−1677.
(49) Wasanasuk, K.; Tashiro, K. Crystal Structure and Disorder in Poly(L-lactic Acid) Delta Form (Alpha′ Form) and the Phase Transition Mechanism to the Ordered Alpha Form. *Polymer* **2011**, *52* (26), 6097−6109.
(50) Kawai, T.; Rahman, N.; Matsuba, G.; Nishida, K.; Kanaya, T.; Nakano, M.; Okamoto, H.; Kawada, J.; Usuki, A.; Honma, N.; Nakajima, K.; Matsuda, M. Crystallization and Melting Behavior of Poly (L-lactic Acid). *Macromolecules* **2007**, *40* (26), 9463−9469.
(51) Zhang, J.; Tashiro, K.; Tsuji, H.; Domb, A. J. Disorder-To-Order Phase Transition and Multiple Melting Behavior of Poly(L-Lactide) Investigated by Simultaneous Measurements of WAXD and DSC. *Macromolecules* **2008**, *41* (4), 1352−1357.
(52) Di Lorenzo, M. L.; Cocca, M.; Malinconico, M. Crystal Polymorphism of Poly(L-lactic acid) and its Influence on Thermal Properties. *Thermochim. Acta* **2011**, *522* (1−2), 110−117.
(53) Lin, Y. J.; Hiltner, A.; Baer, E. Nanolayer Enhancement of Biaxially Oriented Polypropylene Film for Increased Gas Barrier. *Polymer* **2010**, *51* (24), 5807−5814.
(54) Yasuniwa, M.; Tsubakihara, S.; Iura, K.; Ono, Y.; Dan, Y.; Takahashi, K. Crystallization Behavior of Poly(L-lactic acid). *Polymer* **2006**, *47* (21), 7554−7563.
(55) Stoclet, G.; Seguela, R.; Vanmansart, C.; Rochas, C.; Lefebvre, J. M. WAXS Study of the Structural Reorganization of Semi-Crystalline Polylactide under Tensile Drawing. *Polymer* **2012**, *53* (2), 519−528.

(56) Cartier, L.; Okihara, T.; Ikada, Y.; Tsuji, H.; Puiggali, J.; Lotz, B. Epitaxial Crystallization and Crystalline Polymorphism of Polylactides. *Polymer* **2000**, *41* (25), 8909–8919.
(57) Delpouve, N.; Saiter, A.; Mano, J.; Dargent, E. Cooperative Rearranging Region Size in Semi-Crystalline Poly(L-lactic Acid). *Polymer* **2008**, *49*, 3130–3135.
(58) Delpouve, N.; Arnoult, M.; Saiter, A.; Dargent, E.; Saiter, J. M. Evidence of Two Mobile Amorphous Phases in Semicrystalline Polylactide Observed from Calorimetric Investigations. *Polym. Eng. Sci.* **2014**, *54* (5), 1144–1150.
(59) Righetti, M. C.; Gazzano, M.; Delpouve, N.; Saiter, A. Contribution of the Rigid Amorphous Fraction to Physical Ageing of Semi-Crystalline PLLA. *Polymer* **2017**, *125*, 241–253.
(60) Fischer, E.; Sterzel, H.; Wegner, G. Investigation of Structure of Solution Grown Crystals of Lactide Copolymers by Means of Chemical Reactions. *Kolloid Z. Z. Polym.* **1973**, *251*, 980–990.
(61) Bao, D. F.; Liao, X.; He, G. J.; Huang, E. B.; Yang, Q.; Li, G. X. Effects of Enhanced Compatibility by Transesterification on the Cell Morphology of Poly(lactic acid)/ Polycarbonate Blends Using Supercritical Carbon Dioxide. *J. Cell. Plast.* **2015**, *51* (4), 349–372.
(62) Chen, Y.; Peng, Y.; Liu, W. Y.; Zeng, G. S.; Yang, J. H.; Yan, X. H. The Effect of Various Catalyzers on Transesterification in Reactive Blending PC/PLA Blends. *Adv. Mater. Res.* **2013**, *741*, 24–27.
(63) Liu, C.; Lin, S.; Zhou, C.; Yu, W. Influence of Catalyst on Transesterification between Poly(lactic acid) and Polycarbonate under Flow Field. *Polymer* **2013**, *54* (1), 310–319.
(64) Righetti, M. C.; Prevosto, D.; Tombari, E. Time and Temperature Evolution of the Rigid Amorphous Fraction and Differently Constrained Amorphous Fractions in PLLA. *Macromol. Chem. Phys.* **2016**, *217* (18), 2013–2026.